

Article

Impact of Boundary Conditions on a Groundwater Heat Pump System Design in a Shallow and Thin Aquifer near the River

Longcang Shu ^{1,*}, Rui Xiao ¹, Zhonghui Wen ¹, Yuezan Tao ² and Peigui Liu ²

¹ College of Hydrology and Water Resources, Hohai University, Nanjing 210098, China; zhhxr@live.com (R.X.); wenzh2812@sina.com.cn (Z.W.)

² School of Civil Engineering, Heifei University of Technology, Heifei 230009, China; taoyuezan@sohu.com (Y.T.); peiguiliu@yahoo.com.cn (P.L.)

* Correspondence: lcschu@hhu.edu.cn

Academic Editor: Alessandro Franco

Received: 20 April 2017; Accepted: 8 May 2017; Published: 11 May 2017

Abstract: The exploitation of shallow geothermal energy through a groundwater heat pump (GWHP) is always limited to thick and deep aquifers containing abundant water with a relatively stable temperature. Unfortunately, aquifers in hilly regions which occupy two thirds of China are usually thin and shallow. The boundary conditions in those hilly areas affect the groundwater flow that is used for geothermal energy production. To quantify the impact of boundary conditions on the shallow geothermal energy development, a shallow and thin aquifer near the Qingyi River in Anhui Province was chosen as a case study, and a three-dimensional heat–water model was developed using FEFLOW. The impact of the boundary conditions on the hydrodynamic and temperature fields of the aquifer was analyzed by using the developed model. Furthermore, the well locations of a pumping-recharging system near the river correspond to three different modes of pumping-recharging well layouts that were optimized based on the changes of pumping water temperature and the maximum drawdown. The simulation results indicated that the influence of atmospheric temperature on groundwater temperature is negligible below a depth of 11 m. When the river level is above 28 m, the optimal scheme of pumping-only was used (without considering recharging wells) with a certain distance from the river. This scheme not only operates efficiently, but also reduces the operation cost.

Keywords: groundwater heat pump; boundary conditions; numerical model; optimal locations

1. Introduction

Shallow geothermal energy refers to the low-temperature heat energy in groundwater and rock-soil mass at a certain depth below the surface (e.g., buried within 200 m), where the main energy sources are solar radiation and geocentric heat [1]. Recently, the development and utilization of shallow geothermal energy mainly employ the ground source heat pump (GSHP) system. Because of the stable and moderate temperature of the ground, the efficiency of the GSHP system is higher than that of the air source heat pump [2–5]. Now, the GSHP system has been widely accepted as a new technology in the world [6] and has been implemented in 30 countries with an annual increase of 10% [4].

Since the introduction of the theoretical and experimental study of GSHP in the 1990s, the heat pump technology has been developed and employed rapidly in China [7], especially the technology of groundwater heat pumps (GWHPs). The GWHP, among many types of GSHP systems, is one in which energy is extracted from groundwater [8–10]. By the year 1999, 100 GWHP projects had been completed in China, and the total heating supply area reached approximately 1 million m² [11]. Recently, GWHP systems have been widely implemented in almost all provinces in China. The number

of GWHP systems is over 1500, with more than 1800 million m² of heating and cooling areas. The data have shown that GWHP is playing an important role in China [12].

In recent years, scholars have conducted studies on GWHPs focusing on two aspects: reducing the environmental impact of groundwater pumping and improving the heat transfer efficiency of the GWHP system [13]. A commercial building in Rovigo, located in the Po River Plain (Italy), was chosen by Galgaro as a case study [14], and suggested that there are several heating/cooling timetables that reduce the risk of thermal feedback among wells and that these timetables may prevent the GWHP system from becoming uneconomical and energetically inefficient. Händel et al. [9] developed a regional model based on the aquifer at Leibnitzer Feld (Austria), and found the geothermal energy systems in the groundwater have no lasting temperature effects. A coastal aquifer in Southern Italy was chosen as the study area by Masciale [15], and the study demonstrated that the used methodological approach is suitable for the early assessment of the feasibility of the GWHP plant, without affecting the seawater intrusion processes. In Japan, Nam and Ooka conducted a 3D simulation of heat-water transfer according to actual engineering applications, confirming that the condition of the groundwater flow and the position of the wells should be considered when designing a GWHP system [16]. Luo et al. [17] developed a heat transfer model based on a groundwater heat pump project in Nantong, China, and the extent of heat transfixion and land subsidence development was predicted over 10 years of operation. The results showed that a circulation ratio of 60% was the best choice for the sufficient alleviation of heat accumulation, with only limited land subsidence. Zhou et al. [18] analyzed the regularities of heat transfer between pumping and recharging wells, and confirmed that groundwater flow conditions have a great influence on the efficiency of the groundwater heat pump. Gao et al. [19] designed four typical modes of well layouts to determine the thermal interaction influences, and verified their proposed numerical model with a laboratory experiment. As they reported, pumping water temperature changes were associated with the position of the wells, and adopting the row arrangement of well groups may be a better choice compared with others. Lo Russo et al. [20] carried out numerical simulations and a sensitivity analysis for the subsurface parameters influencing the thermally affected zone (TAZ). They reported that the hydrodynamic parameters were highly important in the development of the TAZ. Paksoy et al. [21] adopted CONFLOW progress to quantitatively simulate the transferring feature of the thermal frontal surface in the process of energy abstraction from an aquifer. They studied the optimal distance between the pumping and recharging well groups based on the water level of the pumping wells and the premise of guaranteeing no heat transfixion. The heat transfer model of the two well system developed by Gringarten under a steady-state flow condition was used for assessing thermal breakthrough under various conditions [22].

Previous studies on the development and utilization of shallow geothermal energy have mainly focused on aquifers with abundant groundwater and a stable temperature. These kinds of aquifers are usually distributed throughout the plain regions with a considerable thickness. However, aquifers in hilly regions, which occupy two thirds of China, are usually thinner and shallower compared to plain aquifers. Hydrodynamic and temperature fields of aquifers are easily influenced by the boundary conditions. Therefore, it is necessary to study and develop strategies for using geothermal energy efficiently in those thin and shallow aquifers. So far, researchers have conducted studies on the importance of boundary conditions on solutions of mass and energy transport [23,24]. Similarly, in this paper, we developed a heat-water transfer numerical model according to the shallow and thin aquifer in the first terrace of the Qingyi River and used the model to analyze the influence of boundaries on the hydrodynamic processes and temperature distribution in the aquifer. This study provides a scientific understanding for the further exploitation of geothermal energies in shallow and thin aquifers near rivers.

2. Study Site

The study domain is scoped in Jing County Hospital Building, located in the first terrace of the Qingyi River, Jing County, Anhui Province, China, characterized as a hilly and flat landform, where

towns are generally distributed in the terrace and flood plain. The hospital building has a total floor area of 55,000 m², located near the Southeast Mountain, about 1500 m away from the Qingyi River (Figure 1). An open-loop GWHP system is used for the space heating and cooling of the hospital. Figure 2 shows the meteorological data of mean precipitation and mean temperature at Jing County from 2006 to 2015. The average annual air temperature is 17.93 °C, and the maximum and minimum monthly average temperature occurring in August (30.2 °C) and January (6.02 °C) is demonstrated. The annual mean precipitation over 10 years is about 1505 mm, and the maximum and minimum monthly average rainfalls are 254.5 and 45.3 mm, occurring in June and December, respectively.

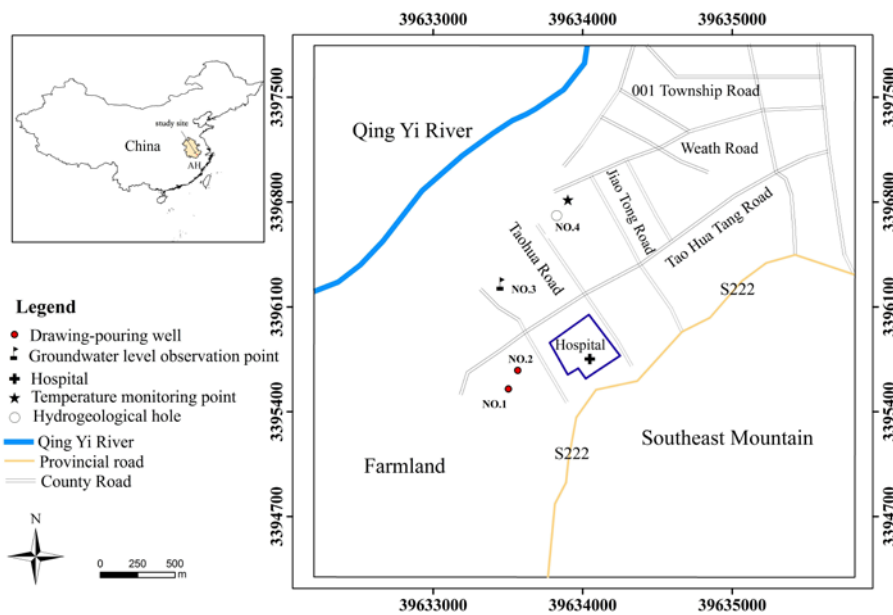


Figure 1. Location of the study site.

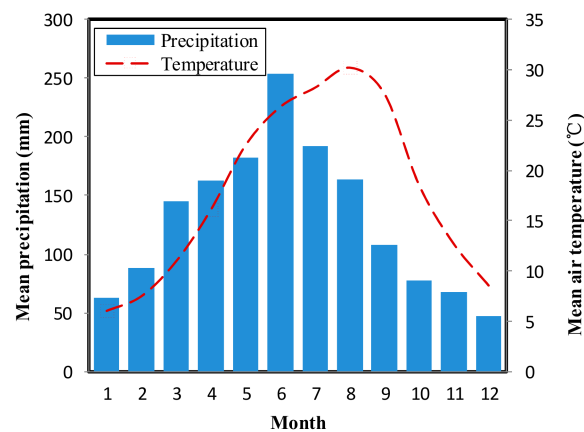


Figure 2. Climatic data of JingXian for 10 years from 2006 to 2015.

In the study area, there are four wells and one temperature monitoring point (Figure 1). The No. 1 and No. 2 Wells are used for pumping tests, while the No. 3 Well is employed for the groundwater level observation and the No. 4 Well is used for the hydrogeological test. According to the borehole log, the strata in the study area can be generally divided into three layers. The first layer is the aquitard consisting of silty clay at a depth of 0–6 m, the second layer is the aquifer consisting of gravels at a depth of 6–16 m, and the third layer is the aquiclude consisting of argillaceous conglomerate below 16 m. The geological cross section shows that the river fully penetrates the phreatic aquifer (Figure 3), and it

can be inferred that the aquifer is hydraulically connected to the Qingyi River. In 2006–2015, the annual mean flow of the Qingyi River was $4.7 \text{ m}^3/\text{s}$, and the minimum river level and the maximum river level was 25.7 m and 31.4 m, respectively.

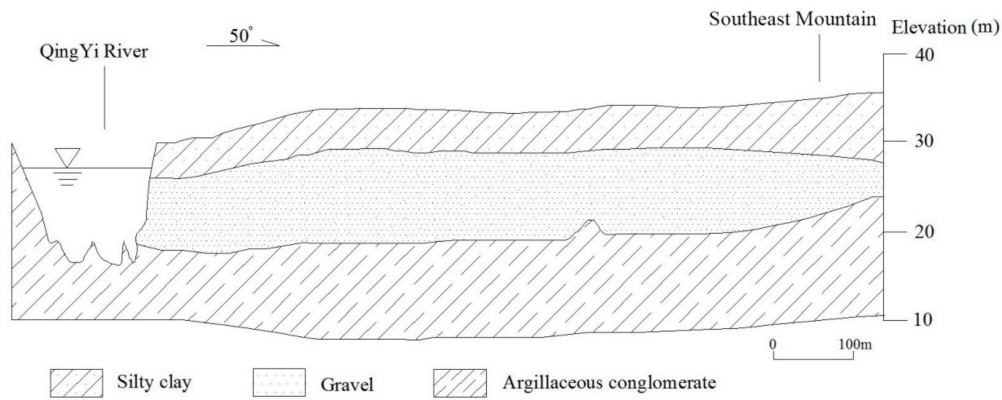


Figure 3. Geological section map of the study site.

Through a double-ring infiltration test and pumping test, the hydraulic conductivity of the unsaturated zone and aquifer were separately determined. The thermal properties of the soil were determined by using previously published data [25–27]. The measurement of the soil and groundwater temperature at various depths was performed by using temperature probes, as shown in Figure 4.

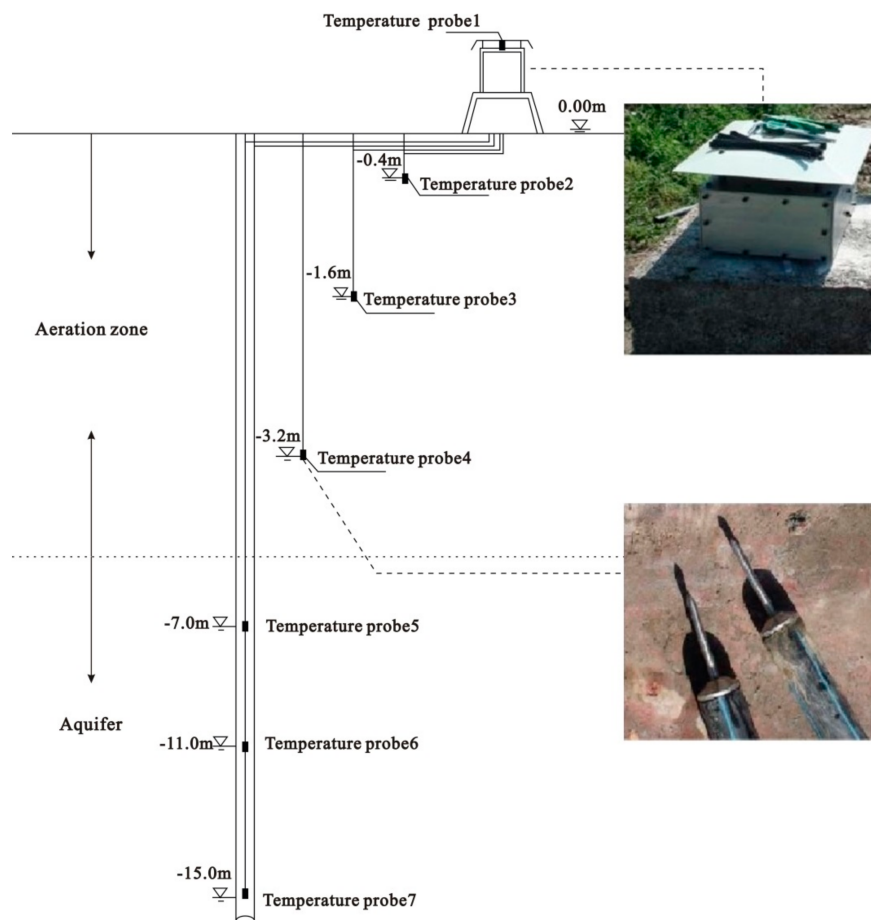


Figure 4. Schematic diagram of the distribution of temperature probes.

3. Numerical Simulation of Groundwater Flow and Heat Transfer

3.1. Numerical Simulation

The influence of the boundary conditions (e.g., air temperature, Qingyi River, as well as precipitation and the Southeast Mountain) on the hydrodynamic processes and temperature distribution in the shallow and thin aquifer was quantified by using the numerical simulation model, which is run using FEFLOW. The mathematical basis of this model is mainly based on the conservation of mass, momentum, and energy [28], as follows:

$$S_0 \frac{\partial(\rho_0 h)}{\partial t} + \frac{\partial(\rho_0 q_i)}{\partial x_i} = Q_p + Q_{EB}(T) \quad (1)$$

$$q_i = -K_{ij} f_\mu \left(\frac{\partial h}{\partial x_j} + \frac{\rho - \rho_0}{\rho_0} e_j \right) \quad (2)$$

$$\frac{\partial}{\partial t} [(\varepsilon \rho_0 c_f + (1 - \varepsilon) \rho_s c_s) T] + \frac{\partial(\rho_0 c_f q_i T)}{\partial x_i} - \frac{\partial}{\partial x_i} (\lambda_{ij} \frac{\partial T}{\partial x_j}) = Q_T \quad (3)$$

where t is time (s); T is temperature ($^{\circ}\text{C}$); x_i and x_j are 3D space variables (m); S_0 is the specific storage (1/m); ε is the effective porosity; q_i is the 3D groundwater flow velocity (m/s); Q_p represents the sources and sinks of groundwater ($\text{kg}/\text{m}^3 \text{ s}$); h is the groundwater head (m); $Q_{EB}(T)$ is the effect of temperature change on flow ($\text{kg}/\text{m}^3 \text{ s}$); K_{ij} is the permeability coefficient (m/s); f_μ is the correction term of the hydraulic conductivity; ρ_0 is the groundwater density (kg/m^3); e_j is the unit vector; c_f and c_s are the specific heat capacities of liquid and solid ($\text{J}/\text{kg } ^{\circ}\text{C}$), respectively; ρ_s is the solid density (kg/m^3); λ_{ij} is the coefficient of thermal conductivity ($\text{W}/\text{m } ^{\circ}\text{C}$); and Q_T is the source-sink term of heat (W/m^3).

3.2. Geological Model Generalization and Discretization

Taking the hospital as the center, the study domain extends 1 km to the northeast and southwest to justify the ambient boundary condition of the model. The Qingyi River and Southeast Mountain are defined as the northwest and southeast boundaries, respectively. The study domain is approximately 4 km². The vertical domain is divided into three layers with distinct hydrogeological and thermal properties based on the hydrogeological borehole data. Meanwhile, according to the vertical distribution position of the temperature probes, the first layer is sub-divided into four layers and the distance from the top of the model to each sublayer is 40, 160, and 320 cm, respectively. The second layer, which represents the aquifer, is sub-divided into three sublayers. Simulations were performed under transient flow and transient transfer conditions using the forward Adams–Bashforth/backward trapezoidal predictor-corrector scheme for automatic time-step control [13]. The hydrogeological and thermal parameters of each layer used for the simulation are shown in Table 1.

Table 1. Model input parameters.

Parameter	Unit	Value		
		Layer 1 (Silty Day)	Layer 2 (Gravel)	Layer 3 (Argillaceous Conglomerate)
Horizontal hydraulic conductivity ($K_{xx} = K_{yy}$)	m/d	0.02	25	0.001
Vertical hydraulic conductivity (K_{zz})	m/d	0.002	2.5	0.0001
Specific storage (S_s)	1/m	0.0001	0.0001	0.0001
Porosity (n)		0.3	0.15	0.01
Thermal conductivity of the solid (λ^s)	W/mk	1.13	1.5	1.4
Thermal conductivity of the fluid (λ^f)	W/mk	0.65	0.65	0.65
Volumetric heat capacity of the solid ($\rho^s c^s$)	MJ/m ³ k	2.09	2.9	1.99
Volumetric heat capacity of the fluid ($\rho^f c^f$)	MJ/m ³ k	4.2	4.2	4.2
Longitudinal thermal dispersivity (α_L)	m	5	5	5
Transverse thermal dispersivity (α_T)	m	0.5	0.5	0.5

3.3. Initial and Boundary Conditions

The initial conditions of the model include two parts: the initial hydrodynamic field and the initial temperature distribution in the aquifer. This study chose 1 January 2015 as the initial time of the simulation. Given that there was no other groundwater exploitation project, the hydrodynamic field of the aquifer maintained its natural state, which can be obtained by linear interpolation based on the measured hydraulic gradient. The highest groundwater level was 30.2 m, and the position of the highest groundwater level was near the Southeast Mountain. The lowest groundwater level was 26.8 m, which was the water level of the Qingyi River on 1 January. The soil and groundwater temperatures at different depths on 1 January was obtained through temperature probes and was then input into the model as the initial temperature distribution in the study domain (Figure 5).

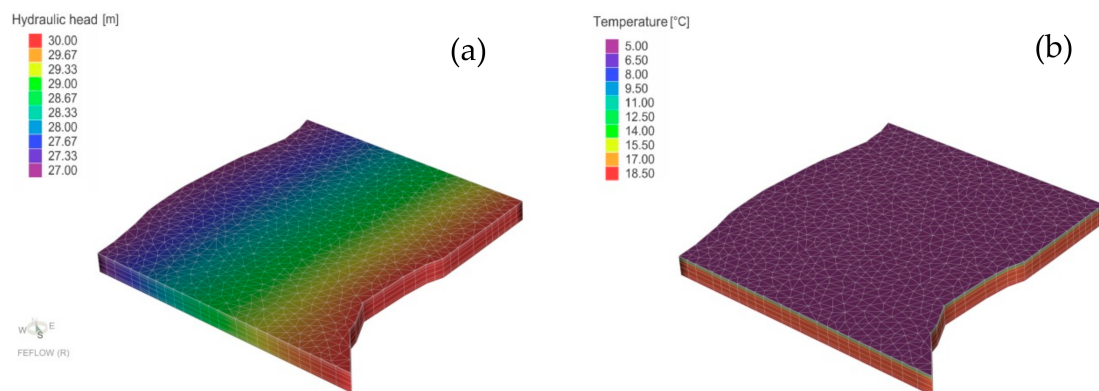


Figure 5. Initial conditions for the analysis of groundwater flow and heat transfer: (a) Hydrodynamic field, (b) Temperature field.

Considering the direct hydraulic connection between the Qingyi River and groundwater, the Qingyi River was set as the Dirichlet boundary condition, and the river level and river water temperature were obtained from the hydrologic station. The mathematical formulation of the river boundary is as follows:

$$H(x, y, z, t)|_{s_1} = \varphi(x, y, z, t), \quad (x, y, z) \in s_1 \quad (4)$$

where H is the river level (m); t is time (s); and $\varphi(x, y, z, t)$ is the known function at boundary s_1 .

Southeast Mountain was defined as the Neumann boundary conditions with zero flux. The southwest and northeast boundaries were set as the Cauchy boundary conditions. The mathematical representation of the boundary condition is as follows:

$$K \frac{\partial H}{\partial n} |_{s_3} = \frac{K_1}{m_1} (H_n - H) = q(x, y, z, t) \quad (5)$$

where K is the permeability coefficient of the aquifer (m/s); K_1 and m_1 are the permeability coefficient (m/s) and thickness (m) of the aquitard, respectively; q is the lateral inflow (m/s); H is the groundwater head at the boundary; H_n is the lateral groundwater head (m); and n is the normal direction of the boundary s_3 .

The air temperature data which was obtained by the temperature measuring instrument was set as the boundary condition on the top of model according to the Equation (6), and the bottom of the model was treated as the impervious boundary condition.

$$T(x, y, z, t)|_{\Gamma_1} = T_1(x, y, z, t) \quad (x, y, z) \in \Gamma_1 \quad (6)$$

where T is the atmospheric temperature ($^{\circ}\text{C}$); t is time (s); and $T_1(x, y, z, t)$ is the known temperature at boundary Γ_1 .

3.4. Design Scheme of the GWHP System

In summer, the recharging water temperature was designed to be 30 °C, and it was designed to be 6 °C in winter. The required total pumping rate for the GWHP system was 198 m³/h according to Equation (7) [29]. Eight pumping wells and eight recharging wells were designed, and the pumping rate of each well was 25 m³/h (Figure 6). The successive operating time of the heat pump during the year was a 60 days heating period (i.e., from January to February) and a 90 days cooling period (i.e., from July to September), in accordance with the climatic characteristics of the study area.

$$Q_f = \frac{Q_h}{\rho \times c_f \times (T_i - T_O)} \quad (7)$$

where Q_f is the pumping rate (m³/s); Q_h is the heating load (W); c_f is the volumetric heat capacity of the pumped groundwater (J/kg °C); ρ is the groundwater density (kg/m³); T_i is the recharging water temperature; and T_O is the pumping water temperature (°C).

To ensure the sufficient water supply for the heat pump and to avoid the drawdown being too large, the recharging wells were laid at the upstream of the groundwater flow field and the pumping wells were laid at the downstream because the pumping-recharging well group was located near the impervious boundary (i.e., the Southeast Mountain), and the thickness of the aquifer was relatively thin. However, the pumping water temperature is heavily influenced by the recharge water, and thermal breakthrough can occur in the well layout above. Therefore, an optimal design for the distance between the pumping well group and the recharging well group is necessary. In this paper, the change of the average pumping water temperature in the three-year heat pump operation period with five different distances between the pumping well group and recharging well group of 60, 90, 120, 150, and 180 m respectively were simulated.

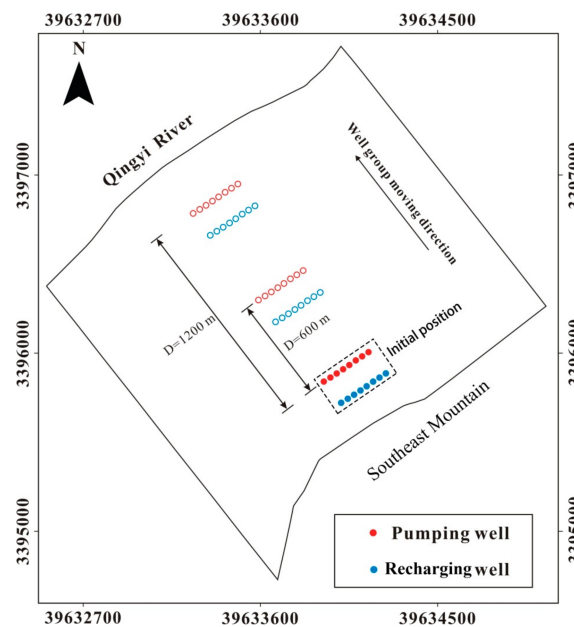


Figure 6. Diagram of the pumping-recharging well group movement.

3.5. River Levels and the Positions of the Pumping-Recharging Well Group

Considering that the river fully penetrates the phreatic aquifer, the change of river level will directly influence the hydrodynamic field and the temperature distribution in the aquifer. Therefore, it is necessary to quantify the impact of the river level on the hydrodynamic field and temperature field of the aquifer. A total of 90 days from 1 July to 31 September in summer were chosen as the simulation

period because the river level changed greatly in summer. The range of the river level was set between 27 and 31 m according to the historical data of the river level. Meanwhile, based on the monitoring data from the hydrologic station in the Qingyi River, the river temperature was set to 24.7 °C, which was the annual mean river water temperature in the summer from 2010 to 2015. In addition, an analysis on the influence of the pumping-recharging well group location on the hydrodynamic field and temperature distribution in the aquifer was also performed. The pumping-recharging well group was moved from the initial position (i.e., $D = 0$ m) towards the river (Figure 6), and the recharge water temperature, pumping capacity, and the distance between the pumping well group and recharging well group remain unchanged. The range of the river level (H) and the moving distance of the pumping-recharging well group (D) used for the analysis are listed in Table 2.

Table 2. Range of variables for analysis.

Variables	Unit	Value
The range of the river level (H)	m	27, 28, 29, 30, 31
Moving distance of well group (D)	m	0, 300, 600, 900, 1200
Distance between well group and river (L)	m	50, 70, 90, 110, 130, 150, 170, 190

Although the river can supply enough water to the heat pump when the pumping-recharging well group moves to the area near the river, the river water temperature will influence the pumping water temperature. Therefore, a further analysis on the influence of the river on the GWHP system was conducted. Three different modes of pumping and recharging well group layouts near the river were implemented for numerical simulation with different distances between the pumping-recharging well group and river (L), in addition to different river levels (H) (Figure 7). The range of the distance between the pumping-recharging well group and river (L) can be seen in Table 2.

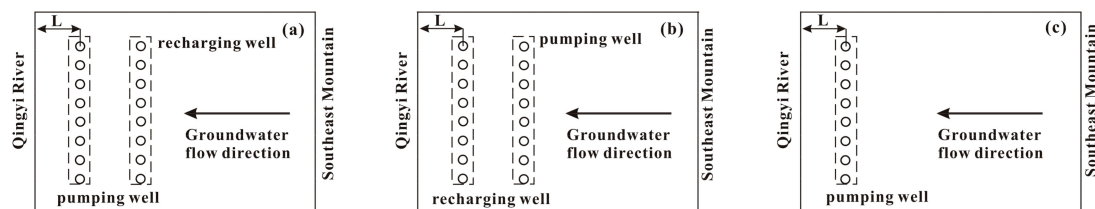


Figure 7. Three modes of the pumping and recharging well group layout. (a) The pumping well group is located downstream of the groundwater flow field and the recharging well group is located upstream of the field; (b) The pumping well group is located upstream and the recharging well group is located downstream of the groundwater flow field; (c) Only the pumping wells were set.

4. Results and Discussion

4.1. Effect of the Atmospheric Temperature

The groundwater level, groundwater temperature, and soil temperature in 2015 were simulated using the developed model and compared with the measurements. In this study, the root mean square error (RMSE)

$$RMSE = \left[\sum_{i=1}^n \frac{(M_i - S_i)^2}{n} \right]^{0.5} \quad (8)$$

was used as a fitness criterion to estimate the quality of fit [30,31] and the acceptable error is estimated to be 5.0% of the measured values [32]. In Equation (8), S_i is the simulated value (i.e., groundwater level, groundwater, and soil temperatures), M_i is the measured value, and n is the number of measurements.

There is good agreement between the simulated results and the measured data (Figures 8 and 9), and the RMSE values of the temperature and groundwater level are 0.46 °C and 0.12 m, respectively,

which are within the acceptable range. As shown in Figure 8, the temperature variation in soil at a depth of 40 cm is greatly influenced by the atmospheric temperature, and the maximum temperature variation is about 26 °C, while the maximum temperature variation in the soil at a depth of 160 cm is 15 °C, and the highest temperature appears at 230 days starting from 1 January 2015. At a depth of 320 cm, the maximum temperature variation in the soil decreases to 7.6 °C, with the highest temperature at 260 days.

In sum, while the variation of soil temperature is inversely dependent of the buried depth, the hysteresis of temperature and depth correlation becomes evident. Moreover, due to the much higher specific heat capacity of water, the impact of atmospheric temperature on the groundwater temperature becomes less than its impact on the soil temperature. At a depth of 7 m, the maximum temperature variation of the groundwater is 1.8 °C under the influence of the surface temperature. However, at a deeper depth (>11 m), the groundwater temperature is almost not affected by the surface temperature and constantly remains at 18 °C (Figure 8). Therefore, the screen of the pumping well should be installed below an 11 m depth to maintain a constant pumping water temperature.

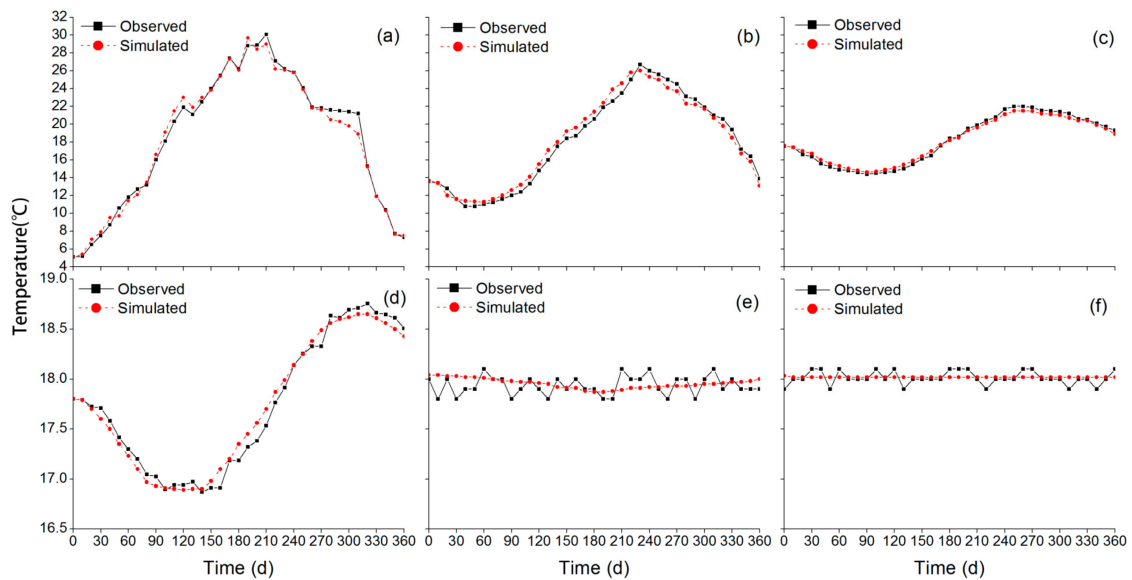


Figure 8. Comparison between observed and simulated temperature at depth of: (a) 0.4 m, (b) 1.6 m, (c) 3.2 m, (d) 7 m, (e) 11 m, and (f) 15 m.

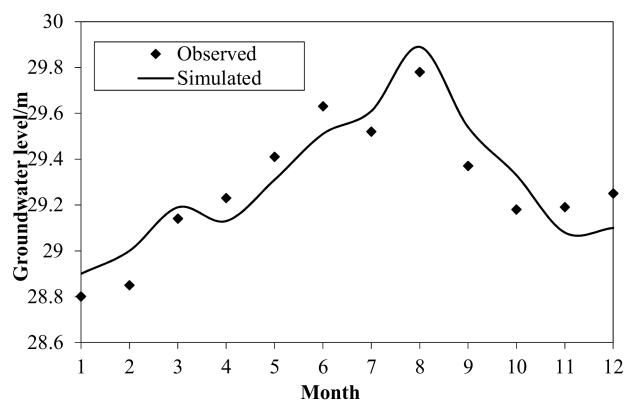


Figure 9. Comparison between the groundwater level measurements and simulation results.

4.2. Optimal Distance between Pumping and Recharging Well Group

The temperature difference between the average pumping water temperature and initial groundwater temperature becomes smaller when the distance between the pumping and recharging well group increases (Figure 10). However, even if the distance increases to 180 m, the maximum variation of the average pumping water temperature is still greater than 1 °C because the aquifer thickness was thin, and the hydraulic conductivity was relatively larger ($K = 25$ m/d). Besides, increasing the distance between the pumping well group and recharging well group requires a larger land area and decreases the recharge efficiency. Therefore, according to the actual conditions of the study site and the performance of the heat pump, the optimal distance between the pumping well group and recharging well group is identified as the corresponding distance when the maximum variation of the average pumping water temperature is less than 2 °C during the GWHP system operation, namely when the grade of thermal interference is below a severe degree [18]. As shown in Figure 10, when the distance between the pumping and recharging well group is 150 m, the maximum temperature difference between the initial groundwater temperature and average pumping water temperature is less than 2 °C, and the operating efficiency of the heat pump can be guaranteed.

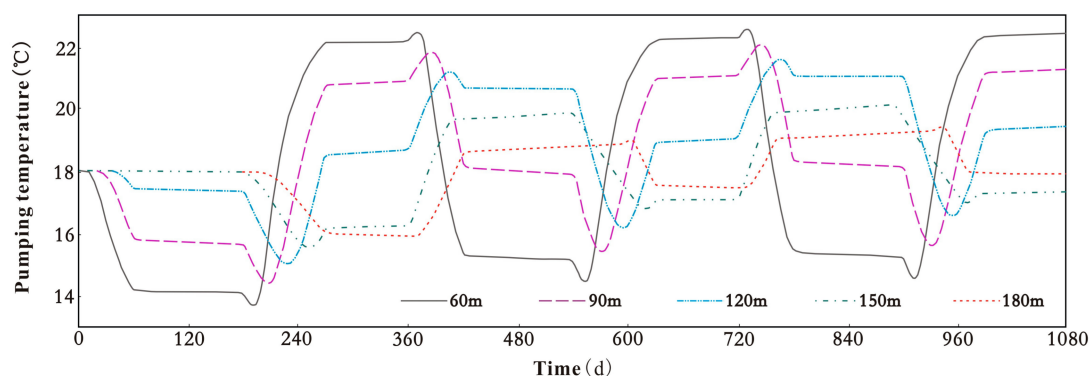


Figure 10. The variation of the average pumping water temperature in the three-year heat pump operation period with five different distances between the pumping and recharging well group.

4.3. Effect of the River Level and the Pumping-Recharging Well Group Location

As shown in Figure 11, the area of the region with drawdown that is larger than 0.5 m decreases gradually when the river level (H) rises and the moving distance of the pumping-recharging well group (D) increases. When the river level rises to 31 m, and the moving distance of the well group reaches 1200 m, the drawdown area is almost 0. As shown in Figure 12, the temperature distribution in the aquifer is almost unaffected by the changes of the river level (H) and the moving distance of the pumping-recharging well group (D), and the area of the region with the change of groundwater temperature being higher than 1 °C basically remains the same. Therefore, it can be concluded that the changes of the river level (H) and the moving distance of the pumping-recharging well group (D) have a greater influence on the hydrodynamic field than on the temperature field of the aquifer.

Figure 13a indicates that the average pumping water temperature at the end of the cooling period decreases with an increase in the moving distance of the pumping-recharging well group (D). Furthermore, when D increases from 0 to 300 m and from 900 to 1200 m, the decreasing trend of the average pumping water temperature is remarkable under the influence of the boundaries.

When the pumping-recharging well group doesn't move (i.e., $D = 0$), the flow of recharging hot water is blocked by the impervious boundary (i.e., Southeast Mountain), and the hot water flows into the pumping well group under the influence of the hydrodynamic field and the pumping action. Therefore, the average pumping water temperature is high. With the increase of D , the effect of thermal accumulation near the Southeast Mountain is gradually weakened, and the average pumping water temperature decreases rapidly.

With the increase of D, part of the river water can flow into the pumping well group. Meanwhile, as shown in Figure 12, the area of the region with the change of groundwater temperature being higher than 1 °C basically remains the same, even though D increases to 1200 m (i.e., about 300 m from river). This indicates that the river water temperature has no influence on the pumping water temperature, and the temperature of the water from the river into the pumping well group is nearly the same with the initial groundwater temperature. Therefore, when D increases from 900 m to 1200 m, the proportion of river water in the total pumping volume grows gradually, and the average pumping water temperature at the end of the cooling decreases quickly. Moreover, the increase in the river level changes the hydraulic gradient between the pumping and recharging well group. Accordingly, the flow velocity of the hot water that travels from the recharging well group towards the pumping well group becomes slower and the average pumping water temperature becomes lower.

Figure 13b indicates that the maximum drawdown at the end of the cooling period decreases in a parabolic trend with D increasing. In addition, the maximum drawdown becomes gradually smaller with the increase of the river level (H). All the corresponding maximum drawdown values at different river levels and different pumping-recharging well group locations are less than 5 m.

Unit:(m)

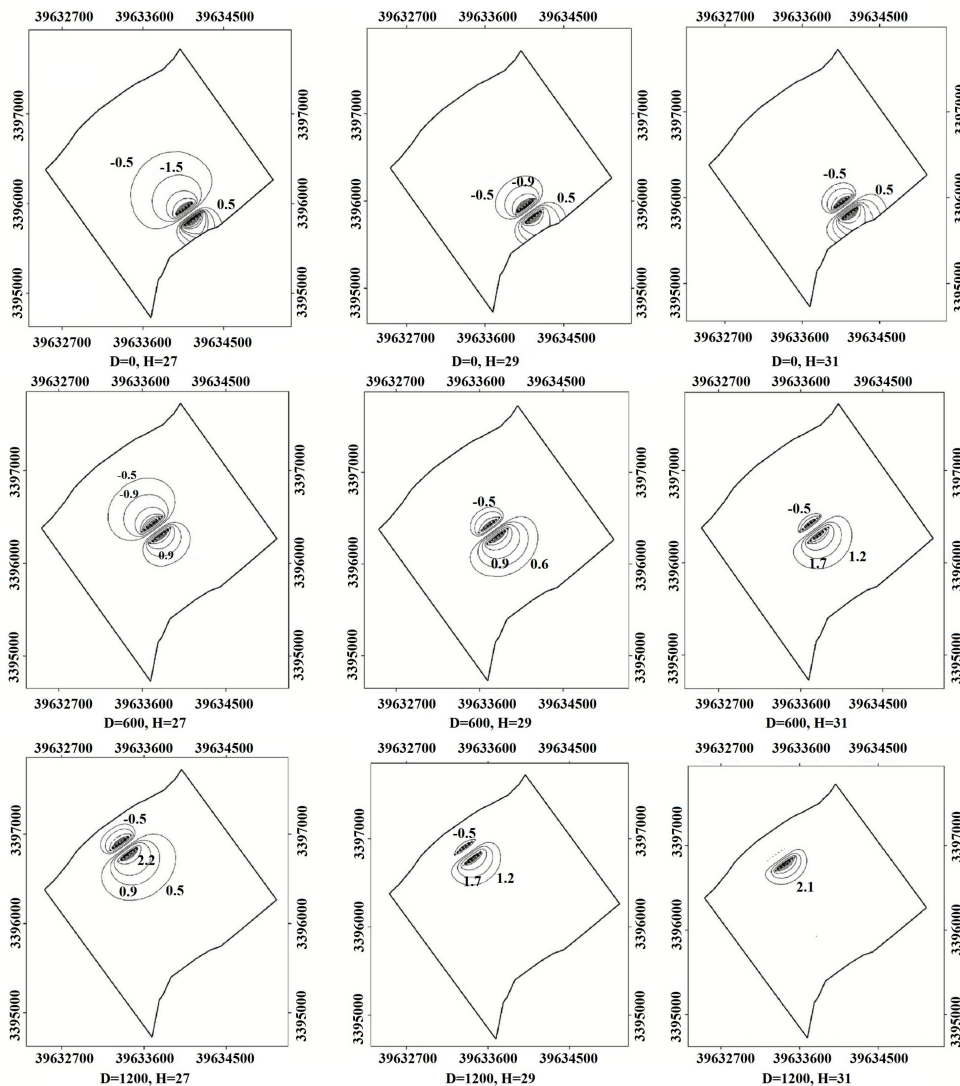


Figure 11. Drawdown contour maps at the end of the cooling period of different river levels and different pumping-recharging well group locations.

Unit:(°C)

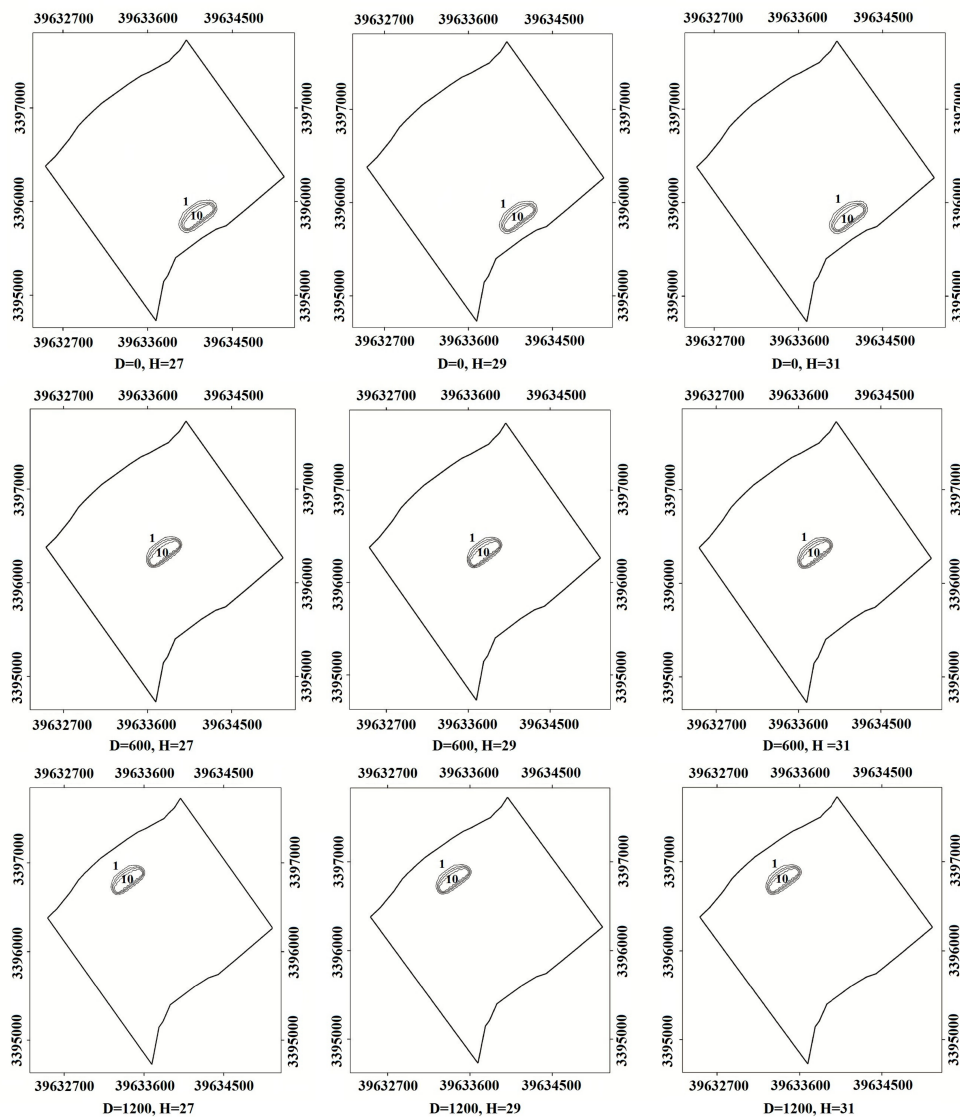


Figure 12. Groundwater temperature variation contour maps at the end of the cooling period of different river levels and different pumping-recharging well group locations.

In summary, when using the GWHP system in the first terrace of river, the pumping-recharging well group should be located near the river for two reasons: Firstly, the pumping water temperature could be decreased at the end of cooling period, so the GWHP system will have a higher heat exchange efficiency. Secondly, the river can supply water to the heat pump and the maximum drawdown could be decreased. However, this summary is based on the premise that the pumping water temperature is not influenced by the river water temperature. Therefore, to further study the influence of the river on the pumping water temperature and the maximum drawdown at the end of summer's cooling period, three different modes of pumping and recharging well group layouts near the river were implemented for numerical simulation.

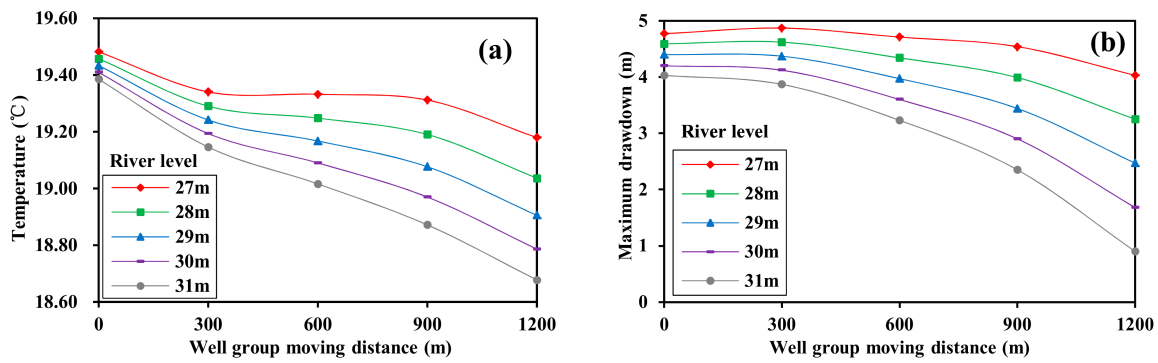


Figure 13. (a) The variation of the average pumping water temperature and (b) the variation of maximum drawdown at the end of the cooling period with different river levels and different moving distances of the pumping-recharging well group.

4.3.1. Mode A

In Mode A, the layout of the wells remains unchanged, namely the pumping well group is located downstream of the groundwater flow field and the recharging well group is located upstream of the field.

Figure 14a shows the relationship between the average pumping water temperature and the distance between the pumping-recharging well group and river (L). When L varies in the range of 50 to 85 m, the average pumping water temperature is high due to the impact of the river water temperature. Moreover, the rise of the river level leads to an increase in the average pumping water temperature, but the rising range of the temperature is small. Besides, the average pumping water temperature decreases quickly in a linear trend with L increasing. When L is in the range of 85 to 190 m, the river water temperature has nearly no influence on the pumping water temperature, and the pumping temperature is mainly affected by the recharge water. The average pumping water temperature increases slowly with L increasing. Meanwhile, the rise of the river level (H) changes the hydraulic gradient and the results in the average pumping water temperature decrease gradually.

Figure 14b indicates that when L increases from 50 to 150 m, the increasing trend of the maximum drawdown is significant. In addition, when L is larger than 150 m, the river boundary has nearly no influence on the hydrodynamic field, and the maximum drawdown becomes relatively stable. Considering that the pumping well group is located downstream of the groundwater flow field and near the river boundary, both the recharging water and river water can flow into the pumping well group. Therefore, the corresponding maximum drawdown values at different river levels are all less than 4 m.

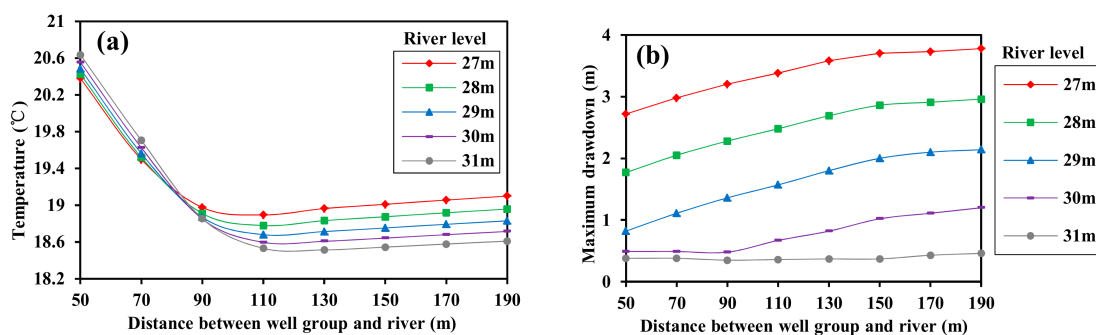


Figure 14. (a) The variation of the average pumping water temperature and (b) the variation of maximum drawdown at the end of cooling period with different river levels and different distances between the pumping-recharging well group and river in Mode A.

4.3.2. Mode B

In Mode B, the layout of the pumping and recharging well group is the reverse to Mode A, namely the pumping well group is located upstream and the recharging well group is located downstream of the groundwater flow field.

Figure 15a shows that the average pumping water temperature at the end of the cooling period increases in a parabolic trend with L increasing. Moreover, the rise of the river level (H) accelerates the flow of the recharge water into the pumping well group and leads to the increase of the average pumping water temperature. Figure 15b indicates that the maximum drawdown becomes smaller with the river level (H) rising. However, the maximum drawdown remains nearly unchanged with L increasing. When the river level is less than 28 m, groundwater recharges the river. Additionally, the pumping well group is located at the upstream of the groundwater flow field, so it causes the maximum drawdown to be larger than 5 m, which is half of the aquifer’s thickness.

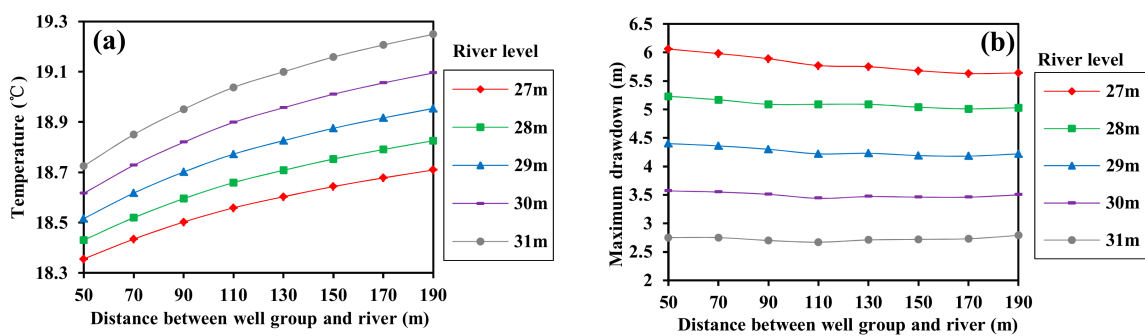


Figure 15. (a) The variation of the average pumping water temperature and (b) the variation of maximum drawdown at the end of the cooling period with different river levels and different distances between the pumping-recharging well group and river in Mode B.

4.3.3. Mode C

When the pumping-recharging well group is located near the river, the river water can flow into the pumping well group to satisfy the water demand of the heat pump. Therefore, the recharging wells will not be set in Mode C.

Figure 16a shows that the average pumping water temperature at the end of the cooling period decreases with L increasing. When L is larger than 170 m, the average pumping water temperature is not affected by the river water and is kept stable at about 18 °C. Figure 16b shows that when L increases, the maximum drawdown grows with a linear trend.

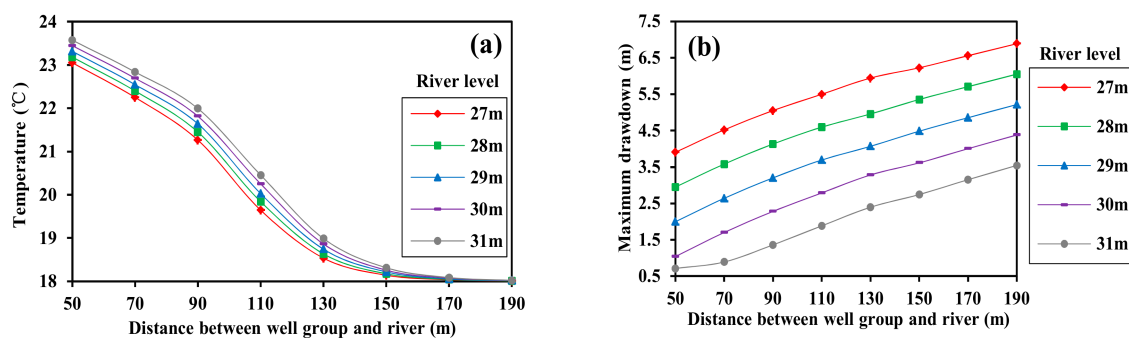


Figure 16. (a) The variation of the average pumping water temperature and (b) the variation of maximum drawdown at the end of the cooling period with different river levels and different distances between the pumping-recharging well group and river in Mode C.

To guarantee that the GWHP system runs efficiently and continuously in the shallow and thin aquifer, not only the efficiency of the heat transfer should be improved, but also the environmental geological problems should be avoided. Therefore, in order to find the optimal location of the pumping-recharging well group, this study sets two restrictive conditions: The first one is that the variation of the average pumping water temperature should be controlled within 1 °C. Namely, if the average pumping water temperature is over 19 °C, we can consider that thermal breakthrough occurred [1]. The second is that the maximum drawdown should be less than half of the aquifer's thickness to avoid the environmental geological problems [33], so the maximum drawdown should be controlled within 5 m in this study. If the pumping temperature and the maximum drawdown satisfy the above two restrictive conditions during the operation of the GWHP system, the location of the pumping-recharging well group can be defined as the optimal pumping-recharging well group location. The optimal locations of the pumping-recharging well group with three modes of well group layouts and different river levels are listed in Table 3.

Table 3. Optimal locations of the well group for three modes of well layouts and different river levels.

Optimal Location (m) Mode	River Level (m)	27	28	29	30	31
	Mode A		88 < L < 144	87 < L < 190	86 < L < 190	86 < L < 190
Mode B				50 < L < 190	50 < L < 147	50 < L < 101
Mode C			123 < L < 131	124 < L < 179	128 < L < 190	129 < L < 190

Table 3 shows that when the river level is 27 m, only Mode A can meet the requirements of the pumping water temperature and maximum drawdown simultaneously. When the river water level rises to 29 m, all three modes of the well group layout display optimal locations. Meanwhile, with the rising of the river level (H), the optimal location of the pumping-recharging well group is almost unchanged for Model A, and it moves toward the river gradually for Model B, while it is gradually further away from the river for Model C.

Although Mode A and Mode C can be selected when the river level is higher than 28 m according to Table 3, priority should be given to Mode C because the recharging well group is not needed in this mode, so it can reduce the operation cost. Moreover, for Mode C, when the river level is higher than 30 m, the average pumping water temperature at the end of the cooling period can be consistent with the initial groundwater temperature when L ranges from 170 to 190 m, and the heat transfer efficiency of the heat pump is maximized.

Considering that the river level in a year changes greatly, the choice of the pumping-recharging well group's location in the actual design of the GWHP system should combine the optimal locations of Mode A with those of Mode C. Therefore, the optimal distance between the pumping-recharging well group and river (L) is identified as being about 130 m, according to Table 3. When the river level is less than 28 m, the pumping well group and recharging well group should run simultaneously according to Mode A, and only the pumping well group needs to run when the river level is higher than 28 m. Through the research of this paper, we can find that using the GWHP system in a specific area near a river may be a better choice compared with the surface-water source heat pump system (SWHPs) [34] because of the relatively stable water temperature and abundant water. Furthermore, the recharging hot water will not be produced when the river level is higher and the GWHP system will not influence the temperature of the river.

In the south of China, the surface water system is developed, and the depth and discharge of the river are generally large. Meanwhile, the annual rainfall is concentrated in the summer, and the river level is relatively high during the cooling period. The structure of the flood plain and the first terrace on the vertical profiles is characterised by a "dual structure", of which the lower part is composed of sand and gravel, and the upper part is sandy loam or clay, so the permeability coefficient of the aquifer near the river is relatively large. Considering that cities are mainly built along the river, there is a high

demand of the cooling or heating load. Therefore, the method mentioned in this paper can be widely used in the region near the southern rivers of China.

5. Conclusions

In this research, a heat–water transfer numerical simulation was developed to study the impact of boundary conditions on the hydrodynamic processes and temperature distribution field in a shallow and thin aquifer near a river. The main conclusions drawn from this paper can be summarized below.

(1) The variation of soil temperature becomes smaller, and the hysteresis of temperature and depth correlation becomes more remarkable, when the depth increases. Although the depth of the aquifer in the study area is shallow, the annual groundwater temperature remained at 18 °C when the depth was more than 11 m.

(2) To ensure sufficient water for the heat pumps, when using the GWHP system in a shallow and thin aquifer, the pumping well group should be located downstream of the groundwater field and the recharging well group should be located upstream of the field. The optimal distance between the pumping and recharging well group for the GWHP system is 150 m.

(3) The changes in the river level and pumping-recharging well group location have a greater influence on the hydrodynamic field than on the temperature field of aquifer. On the premise that the river water temperature has no influence on the pumping water temperature, the average pumping water temperature and maximum drawdown at the end of the summer's cooling period decrease gradually when the river level rises and the moving distance of the pumping-recharging well group increases.

(4) When the river level is above 28 m, the optimal scheme with the pumping well group being used without the recharging well group was proposed with a certain distance from the river. The optimal distance between the pumping-recharging well group and river is identified as being about 130 m. This scheme ensures that the GWHP system runs continually and with a high efficiency. The results of this research can provide a reference for the design of the GWHP system in the shallow and thin aquifers near rivers.

Acknowledgments: This work was supported by the College of Hydrology and Water Resources, Hohai University.

Author Contributions: This research was carried out in collaboration with all authors. Longcang Shu had the original idea for the research. Rui Xiao established the FEFLOW model and finished the calibration and validation work; Zhonghui Wen and Yuezan Tao provided many improvements on the study; Peigui Liu collected the data from the study area.

Conflicts of Interest: The authors declare no conflict of interest.

References

1. Zhang, Q.; Zhang, Y.J.; Gao, P.; Yu, Z.W. Effect of natural cold source on groundwater source heat pump according to laboratory and field geotechnical thermal physical tests. *Energy Build.* **2014**, *84*, 557–566. [[CrossRef](#)]
2. Koochi-Fayegh, S.; Rosen, M.A. On thermally interacting multiple boreholes with variable heating strength: Comparison between analytical and numerical approaches. *Sustainability* **2012**, *4*, 1848–1866. [[CrossRef](#)]
3. Diao, N.; Li, O.; Fang, Z. Heat transfer in ground heat exchangers with groundwater advection. *Int. J. Therm. Sci.* **2004**, *43*, 1203–1211. [[CrossRef](#)]
4. Zhou, X.Z.; Gao, Q.; Chen, X.L.; Yan, Y.Y.; Spitler, J.D. Development status and challenges of GWHP and ATEs in China. *Renew. Sustain. Energy Rev.* **2015**, *42*, 973–985. [[CrossRef](#)]
5. Ramos, E.P.; Breede, K.; Falcone, G. Geothermal heat recovery from abandoned mines: A systematic review of projects implemented worldwide and a methodology for screening new projects. *Environ. Earth Sci.* **2015**, *73*, 6783–6795. [[CrossRef](#)]
6. Lund, J.W.; Freeston, D.H.; Boyd, T.L. Direct utilization of geothermal energy 2010 worldwide review. *Geothermics* **2011**, *40*, 159–180. [[CrossRef](#)]

7. Yang, W.; Zhou, J.; Xu, W.; Zhang, G.Q. Current status of ground-source heat pumps in China. *Energy Policy* **2010**, *38*, 323–332. [[CrossRef](#)]
8. Ferguson, G. Characterizing uncertainty in groundwater-source heating and cooling projects in Manitoba, Canada. *Energy* **2012**, *37*, 201–206. [[CrossRef](#)]
9. Händel, F.; Liedl, R.; Fank, J.; Rock, G. Regional modeling of geothermal energy systems in shallow aquifers: The Leibnitzer Feld case study (Austria). *Environ. Earth Sci.* **2013**, *70*, 3433–3446. [[CrossRef](#)]
10. Liang, J.; Yang, Q.C.; Liu, L.C.; Li, X.Y. Modeling and performance evaluation of shallow ground water heat pumps in Beijing plain, China. *Energy Build.* **2011**, *43*, 3131–3138. [[CrossRef](#)]
11. Zhang, Y.D.; Wan, Y.S. Current status of groundwater source heat pump utilization in China and supervisory suggestions. *China Water Resour.* **2009**, *21*, 39–41.
12. Lin, W.J.; Wu, Q.H.; Wang, G.L. Shallow geothermal energy resource potential evaluation and environmental effect in China. *J. Arid Land Resour. Environ.* **2012**, *26*, 57–61.
13. Park, B.H.; Bae, G.O.; Lee, K.K. Importance of thermal dispersivity in designing groundwater heat pump (GWHP) system: Field and numerical study. *Renew. Energy* **2015**, *83*, 270–279. [[CrossRef](#)]
14. Galgaro, A.; Cultrera, M. Thermal short circuit on groundwater heat pump. *Appl. Therm. Eng.* **2013**, *57*, 107–115. [[CrossRef](#)]
15. Masciale, R.; Carlo, L.D.; Caputo, M.C. Impact of a very low enthalpy plant on a costal aquifer: A case study in Southern Italy. *Environ. Earth Sci.* **2015**, *74*, 1–12. [[CrossRef](#)]
16. Nam, Y.; Ooka, R. Numerical simulation of ground heat and water transfer for groundwater heat pump system based on real-scale experiment. *Energy Build.* **2010**, *42*, 69–75. [[CrossRef](#)]
17. Luo, Z.J.; Wang, Y.; Zhou, S.L.; Wu, X.H. Simulation and prediction of conditions for effective development of shallow geothermal energy. *Appl. Therm. Eng.* **2015**, *91*, 370–376. [[CrossRef](#)]
18. Zhou, X.Z.; Gao, Q.; Chen, X.L.; Yu, M.; Zhao, X.W. Numerically simulating the thermal behaviors in groundwater wells of groundwater heat pump. *Energy* **2013**, *61*, 240–247. [[CrossRef](#)]
19. Gao, Q.; Zhou, X.Z.; Yan, J.; Chen, X.L.; Yan, Y.Y. Numerical simulation of the thermal interaction between pumping and injecting well groups. *Appl. Therm. Eng.* **2013**, *51*, 10–19.
20. Russo, S.L.; Taddia, G.; Verda, V. Development of the thermally affected zone (TAZ) around a groundwater heat pump (GWHP) system: A sensitivity analysis. *Geothermics* **2012**, *43*, 66–74. [[CrossRef](#)]
21. Paksoy, H.O.; Andersson, O.; Abaci, S.; Evliya, H.; Turgut, B. Heating and cooling of a hospital using solar energy coupled with seasonal thermal energy storage in an aquifer. *Renew. Energy* **2012**, *19*, 117–122. [[CrossRef](#)]
22. Gringarten, A.C.; Sauty, J.P.A. Theoretical study of heat extraction from aquifers with uniform regional flow. *J. Geophys. Res.* **1975**, *80*, 4956–4962. [[CrossRef](#)]
23. Lubryka, E.; Malecha, Z.M. The numerical boundary conditions of the wrapping pattern of thin insulation. *Int. J. Heat Mass Transf.* **2017**, *108*, 512–518. [[CrossRef](#)]
24. Malecha, Z.M.; Malecha, K. Numerical analysis of mixing under low and high frequency pulsations at serpentine micromixers. *Chem. Process Eng.* **2014**, *35*, 369–385. [[CrossRef](#)]
25. Chiasson, A.D.; Rees, S.J.; Spitler, J.D. Preliminary assessment of the effects of ground-water flow on closed-loop ground-source heat pump systems. *ASHRAE Trans.* **2000**, *106*, 144–155.
26. Gelhar, L.W.; Welty, C.; Rehfeldt, K.R. A critical review of data on field-scale dispersion in aquifers. *Water Resour. Res.* **1992**, *28*, 1955–1974. [[CrossRef](#)]
27. Molina-Giraldo, N.; Bayer, P.; Blum, P. Evaluating the influence of thermal dispersion on temperature plumes from geothermal systems using analytical solutions. *Int. J. Therm. Sci.* **2011**, *50*, 1223–1231. [[CrossRef](#)]
28. Hans, J.G. *DHI-WASY Software FEFLOW Reference Manual*; DHI WASY GmbH: Berlin, Germany, 2005.
29. Zyoud, S.A.; Rühaak, W.; Sass, I. Dynamic numerical modeling of the usage of groundwater for cooling in north east Jordan—A geothermal case study. *Renew. Energy* **2014**, *62*, 63–72. [[CrossRef](#)]
30. Luo, J.; Rohn, J.; Bayer, M.; Priess, A.; Wei, X. Analysis on performance of borehole heat exchanger in a layered subsurface. *Appl. Energy* **2014**, *123*, 55–65. [[CrossRef](#)]
31. Wagner, V.; Bayer, P.; Kübert, M.; Blum, P. Numerical sensitivity study of thermal response tests. *Renew. Energy* **2012**, *41*, 245–253. [[CrossRef](#)]
32. Sheldon, H.A.; Schaubs, P.M.; Rachakonda, P.K. Groundwater cooling of a supercomputer in Perth, Western Australia: Hydrogeological simulations and thermal sustainability. *Hydrogeol. J.* **2015**, *23*, 1831–1849. [[CrossRef](#)]

33. Zhang, R.; Wu, L.G. *Groundwater Resources Assessment and Management*; Tongji University Press: Shanghai, China, 1997.
34. Chen, X.; Zhang, G.; Peng, J.G.; Liu, T.T. The performance of an open-loop lake water heat pump system in south China. *Appl. Therm. Eng.* **2006**, *26*, 2255–2261. [[CrossRef](#)]



© 2017 by the authors. Licensee MDPI, Basel, Switzerland. This article is an open access article distributed under the terms and conditions of the Creative Commons Attribution (CC BY) license (<http://creativecommons.org/licenses/by/4.0/>).